Open access • Journal Article • DOI:10.1021/ACSNANO.7B04323

Substrate Lattice-Guided Seed Formation Controls the Orientation of 2D Transition-Metal Dichalcogenides — Source link

Areej Aljarb, Zhen Cao, Hao-Ling Tang, Jing-Kai Huang ...+4 more authors

Institutions: King Abdullah University of Science and Technology

Published on: 15 Aug 2017 - ACS Nano (American Chemical Society)

Topics: Monolayer and Molybdenum disulfide

Article

Substrate Lattice-Guided Seed Formation Controls the Orientation of 2D Transition Metal Dichalcogenides

Areej Aljarb, Zhen Cao, Hao-Ling Tang, Jing-Kai Huang, Mengliu Li, Weijin Hu, Luigi Cavallo, and Lain-Jong Li

ACS Nano, **Just Accepted Manuscript** • DOI: 10.1021/acsnano.7b04323 • Publication Date (Web): 07 Aug 2017

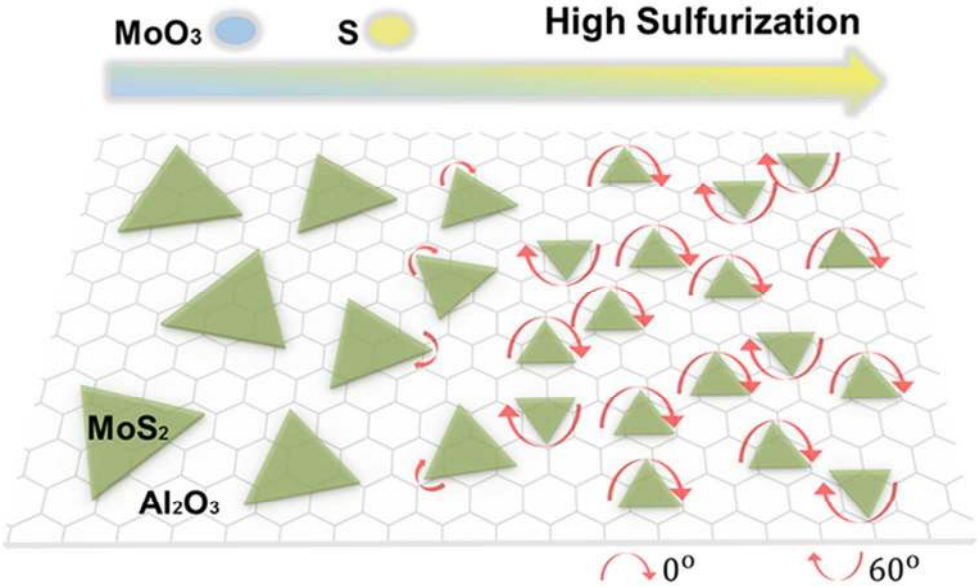

The aligned growth of 2D monolayers is achieved with the controlled orientation of seeds, where a sulfur rich condition is required to minimize the size and define the orientation of seeds.

63x39mm (300 x 300 DPI)

Substrate Lattice-Guided Seed Formation Controls the Orientation of 2D Transition Metal Dichalcogenides

Areej Aljarb, Zhen Cao, Hao-Ling Tang, Jing-Kai Huang, Mengliu Li, Weijin Hu, Luigi Cavallo[*]

and Lain-Jong Li[#*]

King Abdullah University of Science and Technology, KAUST Catalysis Center, Physical Science and Engineering Division, Thuwal 23955-6900, Kingdom of Saudi Arabia.

*To whom correspondence should be addressed: luigi.cavallo@kaust.edu.sa or lance.li@kaust.edu.sa

ABSTRACT

Two-dimensional (2D) transition metal dichalcogenide (TMDCs) semiconductors are important for next-generation electronics and optoelectronics. Given the difficulty in growing large single crystals of 2D TMDC materials, understanding the factors affecting the seed formation and orientation becomes an important issue for controlling the growth. Here, we systematically study the growth of molybdenum disulfide (MoS_2) monolayer on c-plane sapphire with chemical vapor deposition (CVD) to discover the factors controlling their orientation. We show that the concentration of precursors, *i.e.*, the ratio between sulfur and molybdenum oxide (MoO_3), plays a key role in the size and orientation of seeds, subsequently controlling the orientation of MoS_2 monolayers. High S/MoO_3 ratio is needed in the early stage of growth to form small seeds that can align easily to the substrate lattice structures while the ratio should be decreased to enlarge the size of the monolayer at the next stage of the lateral growth. Moreover, we show that the seeds are actually crystalline MoS_2 layers as revealed by high-resolution transmission electron microscopy. There exist two preferred orientations (0° or 60°) registered on sapphire, confirmed by our density functional theory (DFT) simulation. This report offers a facile technique to grow highly aligned 2D TMDCs and contributes to knowledge advancement in growth mechanism.

KEYWORDS: Two-dimensional materials; Molybdenum disulfide (MoS_2); Transition metal dichalcogenides; Chemical vapor deposition; Seeds; Aligned growth.

Two-dimensional (2D) transition metal dichalcogenides (TMDCs) have attracted significant attention owing to their unique electrical,[1-2] optical,[3-5] mechanical[6] and thermal[7] properties inherited from their 2D structures. In clear contrast to the semi-metallic graphene or the unstable black phosphorous,[8] the ambient stable 2D TMDCs demonstrate promising properties for electronic and photoelectronic applications, such as field-effect transistors,[1, 9] sensors,[10-11] solar cells[12] and photodetectors.[3, 13-14] The molybdenum disulfide (MoS_2) monolayer, with a direct energy gap,[15] strong photoluminescence,[16] efficient valley and spin control,[2] is one of the most intensively explored member in the 2D TMDCs family. It can be obtained by mechanical,[17] chemical[18,19] or electrochemical[20] exfoliation. However, these strategies lack uniformity and produce defect-rich samples, which may not be suitable for large-scale device fabrication. For this reason, chemical vapor deposition (CVD) methods using the solid precursors MoO_3 and S powders have been developed.[21]

Nevertheless, the developed CVD methods can not guarantee to synthesize defectless TMDCs with uniform thickness and orientation. The grain boundary between different domains can lower the quality of TMDCs as electronic devices by breaking the structural periodicity and introducing strain defects. Huang *et al.* have further shown that the electronic structures of the grain boundary strongly depends on the misorientation angle of adjacent domains.[22] Hence, recent research efforts have dedicated special attention to control the orientation in order to obtain a large-scale and grain boundary-free monolayer films for higher electron mobility.[23] Owing to the lattice symmetry of the 2D TMDCs layers, they are typically grown as triangles, hexagons or truncated triangles.[24-25] The growth of aligned TMDCs triangles has been achieved on top of other crystalline layered materials such as graphite,[26] graphene[27-29] or boron nitrides,[30] where the TMDC monolayers are either aligned by the graphite step edges or with the substrate lattice through van der Waals (vdW) interaction. The aligned growth has also been

successfully achieved on single crystal substrates with compatible lattice constants such as GaN,[31-32] mica[33] and sapphire.[34-35]

Sapphire has been widely used as a substrate for the growth of 2D TMDC layers owing to its special lattice constant and flat insulating surfaces. Many reports have adopted c-plane sapphire as the substrate for growing TMDC layers.[17,30,31] However, it is known that the sapphire surface can be reconstructed at high temperatures to form long terraces and wide steps.[36] Chen, *et al.* have reported that the step-edges formed on the c-plane sapphire guided the aligned growth of WSe_2,[35] where the alignment became prominent only at the temperatures as high as 950 ^oC. Meanwhile, Dumcenco, *et al.* reported that the key to achieving orientation alignment is the atomically smooth sapphire surfaces, where the sapphire needed to be annealed at a temperature of 1000 ^oC in air for 1 h just before the growth process.[34] However, several other reports did achieve the aligned TMDC triangles without sapphire pre-annealing at such a high temperature prior to the growth.[37] Apparently, the fundamental details of aligned growth are still not yet fully understood. Since many parameters in CVD also affect the growth of TMDCs, such as precursor ratio, pressure, temperature, a systematic study to understand the mechanism of orientation alignment is required. In this study, we report that step-edge or terrace formation on sapphire is not the deterministic factor for the aligned growth of MoS_2. The highly oriented MoS_2 monolayers can be achieved at a much lower temperature (750 ^oC). The higher ratio of sulfur to MoO_3 at the initial nucleation step leads to a relatively smaller size of seeds spontaneously formed on sapphire. Consequently, these small seeds can easily rotate to the energetically favorable position, which is determined by the lattice structure of the substrate, leading to preferred orientation and alignment of TMDCs. By contrast, a lower sulfur to MoO_3 ratio typically results in a larger size of seeds, which loses the capability of orientation control. High-resolution transmission electron microscopy (HRTEM) and energy dispersive X-ray analysis (EDX) reveal that the seeds are also crystalline MoS_2 layers. Density functional theory (DFT) simulations confirm that the small MoS_2 seeds exhibit preferred orientation on

c-plane sapphire. This work provides a fundamental understanding of the seed formation and mechanism for orientation-controlled growth of TMDC monolayer.

RESULTS AND DISCUSSION

Effect of S/MoO_3 precursor ratio on MoS_2 alignment

We adopt the CVD growth process first reported by Lee, *et al.* where the growth of MoS_2 monolayer on sapphire relies on the gas phase reaction of MoO_3 and sulfur vapors carried by a pure Ar flow.[21] Sapphire is commonly used for MoS_2 growth since it is an insulating substrate with high thermal stability and excellent crystalline quality. Additionally, sapphire and MoS_2 both share a hexagonal crystal structure, which makes the growth of TMDCs on sapphire preferable. For this reason, the structure of the sapphire surface plays a key role in determining the MoS_2 orientation through van der Waals (vdW) interaction.[34] It is well known that various surface treatments on sapphire lead to different termination layers on its surfaces, *e.g.,* Al, OH or O termination,[38] which may strongly affect the results of the MoS_2 growth. For our MoS_2 growth, sapphire is first treated with a piranha solution, resulting in OH group termination on the surfaces. Upon heating during the growth, two neighboring Al-OHs shall be dehydrated into Al_2O_3[39] and thus the MoS_2 is grown on the sapphire with an oxygen-terminated surface.

Figure 1a schematically illustrates the growth of MoS_2 layers on c-plane sapphire substrates using the CVD process, and the heating profiles of the precursors sulfur and MoO_3 powders are shown in Figure 1b. Other growth details are provided in the method section. In our typical CVD process, the sulfur powders (at heating zone 1) were first heated to 140 ^oC to fill up the reaction tube with S vapors, followed by the temperature ramping of MoO_3 powders and sapphire substrates (at heating zone 2) to the growth temperature of 800 ^oC as illustrated in the heating profile T_{2A} in Figure 1b. Interestingly, we observe drastically different growth behaviors at different locations of the same sapphire substrate. Figure 1c presents a schematic illustration of how the growth substrate is spatially separated into three

locations. Figure 1d shows the relative concentration of MoO_3 at these locations based on the analysis of our separate experiment which determines the relative concentration of Mo deposits on substrates using EDX (details in supporting materials, Table S1 and Figure S1). The results clearly show that MoO_3 vapor concentration fast decreases with the distance away from the MoO_3 source. Note that in our experiments the sulfur vapor concentration is in excess relative to MoO_3 inside the tube. Hence, our experiments were different from that described by Govind Rajan, *et al.*,[40] where MoO_3 concentration was constant but S concentration decays along the reaction tube. In addition, the diffusivity of sulfur vapors is much higher than that of MoO_3.[41] As a result, the S/MoO_3 ratio significantly increases with distance from the MoO_3 source. The corresponding optical microscope (OM) images for the MoS_2 monolayer flakes growing on these locations are shown in Figure 1e. In location I, the MoS_2 flakes are randomly oriented but they start to show some alignment at location II. In location III, these MoS_2 flakes exhibit dominant edge orientation (0^o and 60^o as detailed in the statistical analysis in supporting information Figure S2). The effect is not caused by the temperature variations since the temperatures at these locations are the same (within the range of $\pm$ 1 ^oC). In previous reports, incrementing the S/MoO_3 ratio results in the geometry of the produced MoS_2 shifting from hexagon to triangle.[24-25, 40] Our experiments always produce triangular MoS_2 flakes, indicating the excess amount of sulfur vapor in the reaction tube. Besides, our experimental results clearly correlate the S/MoO_3 vapor ratio to the orientation control. We hypothesize that at high S/MoO_3 ratio the sulfur vapors efficiently reduce the MoO_3 to form small MoS_2 crystalline seeds, which have the ability to rotate and align with the lattice structure of the substrate. By contrast, low S/MoO_3 ratio may result in the incomplete sulfurization of MoO_3, with relatively larger and thicker seeds. These sub-oxide nanoparticles may land on the sapphire substrate randomly. Consequently, the synthesized MoS_2 flakes exhibit random orientations.

Growth of aligned MoS_2 monolayers with a seeding step

Since a sulfur-rich environment is essential to form small MoS_2 seeds as hypothesized above, the two-step heating profile T_{2B} (shown in Figure 1b) is designed to achieve better alignment across the whole

sample regions (including locations I, II and III), where the substrate first stay at 750 ^{o}C for 5 min before it is heated to the growth temperature. This step ensures a highly S-rich environment for completing the sulfurization of slightly evaporated MoO_3 at the seed formation stage. Consequently, very small seeds can form and rotate easily to stay at a more energetically favorable orientation on the substrate. Although growing MoS_2 flakes can be very slow at 750 ^{o}C due to insufficient MoO_3 vapors, extending the growth time results in small monolayers with edge lengths less than 1 μm as shown in Figure S3. This observation is consistent with Pan *et al.,* where they revealed that at the low temperature of 750 °C tiny monolayers on Si substrate were obtained.[42] Therefore, we designed a profile where after aligning small seeds at 750 °C, the temperature is increased to 800 ^{o}C to increase the lateral growth and enlarge the monolayers size. Gratifyingly, we observed that all regions including I, II and III are grown with aligned MoS_2 monolayers, see Figure 2. Figure 2a shows the typical OM images of the MoS_2 monolayer flakes grown at the central region II using the heating profiles T_{2B}, where the MoS_2 flakes are highly aligned and the dominant edge orientations are 0^{o} and 60^{o} as illustrated by the statistical analysis in Figure 2b. For comparison, one selected typical OM image for the MoS_2 monolayers growth with the typical T_{2A} profile (region II) is shown in Figure 2c and the corresponding statistical orientation analysis in Figure 2d clearly demonstrates the feature of random orientation. We have also performed separate experiments to examine the importance of the sulfur rich condition on MoS_2 alignment by changing the feeding time of sulfur. The results in Figure S4 show that early feeding of S vapors results in better orientation alignment, strongly corroborating our hypothesis.

At a high temperature, c-plane sapphire would usually develop terrace structures with atomic steps on the surface. Aligned growth as guided by those steps has been reported for WSe_2 on sapphire, where the growth temperature was above 950 ^{o}C.[35] However, in our case the growth temperature of 800 ^{o}C is not sufficiently high to conduct step edge-guided aligned growth. Consequently, our growth orientation is controlled by lattice crystal structure of the substrates instead of the terraces. Figure 2e shows an atomic

force microscope (AFM) image for a monolayer MoS_2 grown by our process on a sapphire substrate, where the edge of the flake is clearly not aligned with the steps from terrace structures.

Structure of the seeds

To explore the structure of the seeds, the growth is stopped after the seed formation stage (750 ^oC for 5 min in a sulfur-rich environment). AFM is adopted to characterize the morphology and size of the seeds initiated at this stage. Figure 3a is a typical AFM image for the seeds formed at the upstream side of the reaction zone. The shape of the seeds is identified as a triangle (more AFM images of the MoS_2 seeds are provided in supporting information Figure S5). Unlike the results for one-step heating profile, the triangles in the upstream are aligned since the two-steps heating profile results in small seeds in all the substrate locations which can rotate and align to the substrate. Figure 3b shows the cross-sectional height profile for the seed along the dashed line in Figure 3a, given a thickness of ~0.6 nm monolayer which agrees well with the reported thickness of MoS_2 monolayers.[43] Figure 3c displays the AFM image for the seeds formed at the downstream side with a thickness ~1.2 nm (Figure 3d). The seeds at downstream side are normally with an apparent size of 20-30 nm. Note that the size may be overestimated since the lateral size measurement is limited by the size of the AFM tip end. Hence, identifying the shape of the seed is challenging. The size difference of the seeds in different regions may be related to the amount of the MoO_3 vapor reaching the regions. It would require future investigations.

Most of the as-grown MoS_2 monolayers do not exhibit identifiable nucleation center in the middle of the triangles under OM observation. However, we still occasionally find thick seeds with a pyramid shape as shown in Figure 4a. The cross-sectional HRTEM image in Figure 4b confirms these thick seeds consist of stacked MoS_2 layers, indicating even larger MoO_3 can be completely sulfurized to form MoS_2. The thickness is measured to be 7.5 nm corresponding to around 10 layers of MoS_2. Additionally, Figure 4c shows the energy dispersive X-ray analysis (EDX) images for Al, O, Mo and S signals at the same location in Figure 4b. No O is observed in the MoS_2 multilayers, which again confirms that the

seed is composed of stacked MoS_2 and the precursor MoO_3 is completely sulfurized at the seed formation stage.

Density functional theory simulation

A more detailed investigation from the atomic viewpoint was performed through density functional theory (DFT) calculations. A model consisting of 4×4 unit cells of Al_2O_3 and 6×6 MoS_2 was constructed to minimize the lattice constant mismatch to 0.7%. As described, we believe the MoS_2 monolayer is deposited on the sapphire c-plane with oxygen terminations, which is in clear contrast to the previously proposed models using the sapphire terminated with H or Al.[34] After optimization (Figure 5a), the vertical distance between the upper sulfur of MoS_2 and the sapphire surface is 5.8 Å, which is comparable with our AFM characterization.

Since the seed only contains Mo and S, it is represented by a more prototypical hexagon MoS_2 piece as shown in Figure 5b. A systematic scanning consisting of over 7000 calculations with fixed relative orientations and positions between the MoS_2 seed and Al_2O_3 substrate were performed, thereafter, to evaluate potential energy surface (PES) as a function of the relative position and orientation between the MoS_2 seed and the sapphire substrate. Due to the heavy computational load, the distance between the top O layer of Al_2O_3 and the top S layer of MoS_2 was fixed at 5.8 Å, which is the distance obtained from structural optimization. Figure 5c gives a description of the PES corresponding to an angle of 0°, and the other maps are shown in Figure S6. We have scanned large enough area to cover the Al_2O_3 surface region, and the distance between the maxima and minima of the PES is consistent with the distance between oxygen atoms at c-plane, indicating that the vdW interaction can tune the relative position of the MoS_2 seeds landing on the surface. Thereafter, the configurations corresponding to the minimum in this PES is chosen for orientation scans of the MoS_2 seed. For each specific orientation, the relative positions were also scanned to get a complete view of the PES. The representative configurations for each orientation were chosen from the minimum of the PES, and the energies were calculated with a higher precision (details in supporting materials). We obtain relative energy as a function of orientation

angles with the most favorable position of the MoS_2 seed as shown in Figure 5d. Considering the symmetry feature of our model, the results corresponding to 0~60 degree relative orientation were demonstrated in this report.

Even though we simplify the simulation by using this small hexagon seed without considering the structural variation induced by a high experimental temperature, the simulation can give consistent trend compared with experiments: the 0^o or 60^o configurations are most favorable. It is also of interest to obtain further insights from this model. For instance, the PES is quite smooth and does not have large kinetic barriers (~5 kBT for experimental temperature), indicating the seed can smoothly find its energetic minimum. Consequently, in our experiment, a 5-minute plateau at 750 ^oC (Figure 1b) plays a role in assisting the small seeds finding their favorable configurations. Besides, any treatment destroying this smooth PES by generating additional large energy barriers may bring troubles by kinetically trapping the seed into a local minimum. In short, relatively flat substrate surface having periodic energetic minimums without significant energy barriers can be suitable to template the seed and generate highly aligned TMDC monolayers.

CONCLUSION

In conclusion, we have synthesized highly oriented MoS_2 monolayers by controlling the sulfurization of MoO_3 using CVD method. It is concluded that high sulfurization in the seed formation stage plays an important role to form a small seed, which can easily align with the lattice structure of the sapphire substrate. Seeds can be grown at 750 ^oC, whereas higher temperature 800 ^oC speeds up the lateral growth. Additionally, we provide evidence that the seed is completely sulfurized and consists of MoS_2. Such orientation control can be applicable for other 2D TMDC growth on a crystalline substrate. It is anticipated that such understanding of growth mechanism is crucially important for controlling the growth of diverse 2D materials and further understanding the aligning mechanism of TMDC growth on other hexagonal surfaces such as TMDC, BN, graphene and graphite heterostructure or single crystal substrates with compatible lattice constants such as GaN and mica.

MATERIALS AND METHODS

Chemical Vapor Deposition of TMDCs. The MoS_2 monolayer was grown by the chemical vapor deposition method. The precursors are MoO_3 (Sigma-Aldrich, ≥ 99.5% purity) and S (Sigma-Aldrich, ≥99.5% purity) powders. The sulfur powder (4 g) was put at the upper stream side of the furnace (heating zone 1), and the temperature was maintained at 140 °C during the reaction. In the heating zone 2, center of the reaction chamber, the MoO_3 powder (0.8 g) was placed in a ceramic boat with a 1 cm × 5 cm sapphire substrate placed at the downstream of the ceramic boat. The gas flow was from Ar (Ar = 90 sccm) and the chamber pressure was controlled at 40 Torr. First, the center of the furnace was gradually heated from room temperature to 750 °C at a ramping rate of 25 °C/min and kept at this temperature for 5 min. Then, the temperature was increased to the growth temperature 800 °C with the same ramping rate and kept for 10 min. The furnace was then naturally cooled to room temperature. The consumption rate for S and MoO_3 is estimated as 1.69 mg/min and 0.88 mg/min respectively (Sulfur-rich reaction condition).

Characterization. Optical Images were collected using a Witec alpha 300 confocal Raman microscope with a RayShield coupler. The Mo concentration was analysed using scanning electron microscopy (SEM) imaging and energy dispersive X-ray (EDX) spectra which conducted using FEI Quanta 600 EDAX operating at 10 kV. The seeds and surface morphologies were examined on a commercial multifunction AFM instrument (Cypher ES model from Asylum Research Oxford Instruments) operating in contact mode. Olympus (OMCL-AC240TS) Al-coated silicon cantilevers were used for AFM characterizations. The resonance frequency was ~70 kHz; the spring constant was ~2 N/m, and the tip curvature radius was ~7 nm. The TEM cross-sectional samples were prepared in a Helios NanoLab 660 DualBeam FIB(focus ion Beam) system. Cross section HRTEM imaging and energy dispersive X-ray (EDX) spectrum mapping data were conducted using FEI TITAN AND OSIRIS operating at 300 kV and 200kV respectively.

Density Functional Theory Modeling. The calculations started from the optimization of an Al_2O_3 slab consisting of 4 by 4 unit cells with 5 layers of oxides. The optimization were performed using the RPBE functional[44] and the projected-augmented plane-wave method[45] using the VASP package.[46] The vdW interactions were described through Grimme's correction.[47] The energy cutoff was chosen as 400 eV. The energy convergence criteria was chosen as $1.0x10^{-6}$ eV, and the force convergence criteria was chosen as $1.0x10^{-2}$ eV/Å. Due to the computational load, the scanning process for the PES with different orientation angles uses 1x1x1 k point (at the Γ point), while the energy calculation for the chosen configurations uses 4x4x2 k points using a Monkhorst-Pack grid. The scanning for Figure 5a is performed at a 0° fixed angle over a 7×7 Å^2 region with a 0.2 Å grid length to cover larger area (longer than the terminal oxygen-oxygen distance). The scanning for other angles is to find the nearby energy minima, therefore, only cover a smaller 3×3 Å^2 area with the 0.1 Å grid length.

ACKNOWLEDGMENT All authors acknowledge support from King Abdullah University of Science and Technology (KAUST) under Competitive Research Grant (#CRG4-2634) and KAUST Catalyst Center, Saudi Arabia. The simulations were performed on the Shaheen II supercomputer.

Supporting Information Available: Table S1 and Figures S1-S6 are included. This material is available free of charge *via* the Internet at http://pubs.acs.org.

REFERENCES AND NOTES

1. Radisavljevic, B.; Radenovic, A.; Brivio, J.; Giacometti, i. V.; Kis, A., Single-Layer MoS_2 Transistors. *Nat. Nanotechnol.* **2011,** *6*, 147-150.

2. Zeng, H.; Dai, J.; Yao, W.; Xiao, D.; Cui, X., Valley Polarization in MoS_2 Monolayers by Optical Pumping. *Nat. Nanotechnol.* **2012**, *7*, 490-493.

3. Lopez-Sanchez, O.; Lembke, D.; Kayci, M.; Radenovic, A.; Kis, A., Ultrasensitive Photodetectors Based on Monolayer MoS_2. *Nat. Nanotechnol.* **2013**, *8*, 497-501.

4. Zhang, W.; Chuu, C.-P.; Huang, J.-K.; Chen, C.-H.; Tsai, M.-L.; Chang, Y.-H.; Liang, C.-T.; Chen, Y.-Z.; Chueh, Y.-L.; He, J.-H., et al., Ultrahigh-Gain Photodetectors Based on Atomically Thin Graphene- MoS_2 Heterostructures. *Sci. Rep.* **2014**, *4*, 3826.

5. Cong, C.; Shang, J.; Wu, X.; Cao, B.; Peimyoo, N.; Qiu, C.; Sun, L.; Yu, T., Synthesis and Optical Properties of Large - Area Single - Crystalline 2D Semiconductor WS_2 Monolayer from

Chemical Vapor Deposition. *Adv. Opt. Mater.* **2014**, *2*, 131-136.

6. Bertolazzi, S.; Brivio, J.; Kis, A., Stretching and Breaking of Ultrathin MoS_2. *ACS Nano* **2011**, *5*, 9703-9709.

7. Cai, Y.; Lan, J.; Zhang, G.; Zhang, Y.-W., Lattice Vibrational Modes and Phonon Thermal Conductivity of Monolayer MoS_2. *Phys. Rev. B* **2014**, *89*, 035438.

8. Lin, S.; Chui, Y.; Li, Y.; Lau, S. P., Liquid-Phase Exfoliation of Black Phosphorus and Its Applications. *FlatChem* **2017**, *2*, 15-37.

9. Das, T.; Ahn, J.-H., Development of Electronic Devices Based on Two-Dimensional Materials. *FlatChem* **2017**, *3*, 43-63.

10. Perkins, F. K.; Friedman, A. L.; Cobas, E.; Campbell, P.; Jernigan, G.; Jonker, B. T., Chemical Vapor Sensing with Monolayer MoS_2. *Nano Lett.* **2013**, *13*, 668-673.

11. Li, H.; Yin, Z.; He, Q.; Li, H.; Huang, X.; Lu, G.; Fam, D. W. H.; Tok, A. I. Y.; Zhang, Q.; Zhang, H., Fabrication of Single‐and Multilayer MoS_2 Film‐Based Field‐Effect Transistors for Sensing No at Room Temperature. *Small* **2012**, *8*, 63-67.

12. Van Le, Q.; Choi, J.-Y.; Kim, S. Y., Recent Advances in the Application of Two-Dimensional Materials as Charge Transport Layers in Organic and Perovskite Solar Cells. *FlatChem* **2017**, *2*, 54–66.

13. Zhang, W.; Huang, J. K.; Chen, C. H.; Chang, Y. H.; Cheng, Y. J.; Li, L. J., High-Gain Phototransistors Based on a CVD MoS_2 Monolayer. *Adv. Mater.* **2013**, *25*, 3456-3461.

14. Yin, Z.; Li, H.; Li, H.; Jiang, L.; Shi, Y.; Sun, Y.; Lu, G.; Zhang, Q.; Chen, X.; Zhang, H., Single-Layer MoS_2 Phototransistors. *ACS Nano* **2011**, *6*, 74-80.

15. Mak, K. F.; Lee, C.; Hone, J.; Shan, J.; Heinz, T. F., Atomically Thin MoS_2: A New Direct-Gap Semiconductor. *Phys. Rev. Lett.* **2010**, *105*, 136805.

16. Splendiani, A.; Sun, L.; Zhang, Y.; Li, T.; Kim, J.; Chim, C. Y.; Galli, G.; Wang, F., Emerging Photoluminescence in Monolayer MoS_2. *Nano Lett.* **2010**, *10*, 1271–1275.

17. Li, H.; Wu, J.; Yin, Z.; Zhang, H., Preparation and Applications of Mechanically Exfoliated Single-Layer and Multilayer MoS_2 and WSe_2 Nanosheets. *Acc. Chem. Res.* **2014**, *47*, 1067-1075.

18. Eda, G.; Yamaguchi, H.; Voiry, D.; Fujita, T.; Chen, M.; Chhowalla, M., Photoluminescence from Chemically Exfoliated MoS_2. *Nano Lett.* **2011**, *11*, 5111-5116.

19. Ortiz-Quiles, E. O.; Cabrera, C. R., Exfoliated Molybdenum Disulfide for Dye Sensitized Solar Cells. *FlatChem* **2017**, *2*, 1-7.

20. Zeng, Z.; Yin, Z.; Huang, X.; Li, H.; He, Q.; Lu, G.; Boey, F.; Zhang, H., Single-Layer Semiconducting Nanosheets: High‐Yield Preparation and Device Fabrication. Angew. *Chem., Int. Ed* **2011**, *50*, 11093-11097.

21. Lee, Y. H.; Zhang, X. Q.; Zhang, W.; Chang, M. T.; Lin, C. T.; Chang, K. D.; Yu, Y. C.; Wang, J. T. W.; Chang, C. S.; Li, L. J., Synthesis of Large-Area MoS_2 Atomic Layers with Chemical Vapor Deposition. *Adv. Mater.* **2012**, *24*, 2320-2325.

22. Huang, Y. L.; Chen, Y.; Zhang, W.; Quek, S. Y.; Chen, C.-H.; Li, L.-J.; Hsu, W.-T.; Chang, W.-H.; Zheng, Y. J.; Chen, W., Bandgap Tunability at Single-Layer Molybdenum Disulphide Grain Boundaries. *Nat. Commun.* **2015**, *6*, 6298.

23. Najmaei, S.; Amani, M.; Chin, M. L.; Liu, Z.; Birdwell, A. G.; O'Regan, T. P.; Ajayan, P. M.; Dubey, M.; Lou, J., Electrical Transport Properties of Polycrystalline Monolayer Molybdenum Disulfide. *ACS Nano* **2014**, *8*, 7930-7937.

24. Yang, S. Y.; Shim, G. W.; Seo, S.-B.; Choi, S.-Y., Effective Shape-Controlled Growth of Monolayer MoS_2 Flakes by Powder-Based Chemical Vapor Deposition. *Nano Res.* **2017**, *10*, 255-262.

25. Wang, S.; Rong, Y.; Fan, Y.; Pacios, M.; Bhaskaran, H.; He, K.; Warner, J. H., Shape Evolution of Monolayer MoS_2 Crystals Grown by Chemical Vapor Deposition. *Chem. Mater.* **2014**, *26*, 6371-6379.

26. Lu, C.-I.; Butler, C. J.; Huang, J.-K.; Hsing, C.-R.; Yang, H.-H.; Chu, Y.-H.; Luo, C.-H.; Sun, Y.-C.; Hsu, S.-H.; Yang, K.-H. O., Graphite Edge Controlled Registration of Monolayer MoS_2 Crystal Orientation. *Appl. Phys. Lett.* **2015**, *106*, 181904.

27. Lin, Y.-C.; Lu, N.; Perea-Lopez, N.; Li, J.; Lin, Z.; Peng, X.; Lee, C. H.; Sun, C.; Calderin, L.; Browning, P. N., Direct Synthesis of Van Der Waals Solids. *ACS Nano* **2014**, *8*, 3715-3723.

28. Ago, H.; Endo, H.; Solís-Fernández, P.; Takizawa, R.; Ohta, Y.; Fujita, Y.; Yamamoto, K.; Tsuji, M., Controlled Van Der Waals Epitaxy of Monolayer MoS_2 Triangular Domains on Graphene. *ACS Appl. Mater. Interfaces* **2015**, *7*, 5265-5273.

29. Ago, H.; Fukamachi, S.; Endo, H.; Solís-Fernández, P.; Mohamad Yunus, R.; Uchida, Y.; Panchal, V.; Kazakova, O.; Tsuji, M., Visualization of Grain Structure and Boundaries of Polycrystalline Graphene and Two-Dimensional Materials by Epitaxial Growth of Transition Metal Dichalcogenides. *ACS Nano* **2016**, *10*, 3233-3240.

30. Yu, H.; Yang, Z.; Du, L.; Zhang, J.; Shi, J.; Chen, W.; Chen, P.; Liao, M.; Zhao, J.; Meng, J., Precisely Aligned Monolayer MoS_2 Epitaxially Grown on H‐Bn Basal Plane. *Small* **2016**, *13*, 1603005.

31. Ruzmetov, D.; Zhang, K.; Stan, G.; Kalanyan, B.; Bhimanapati, G. R.; Eichfeld, S. M.; Burke, R. A.; Shah, P. B.; O'Regan, T. P.; Crowne, F. J., et al., Vertical 2d/3d Semiconductor Heterostructures Based on Epitaxial Molybdenum Disulfide and Gallium Nitride. *ACS Nano* **2016**, *10*, 3580-3588.

32. Chen, Z.; Liu, H.; Chen, X.; Chu, G.; Chu, S.; Zhang, H., Wafer-Size and Single-Crystal $MoSe_2$ Atomically Thin Films Grown on Gan Substrate for Light Emission and Harvesting. *ACS Appl. Mater. Interfaces* **2016**, *8*, 20267-20273.

33. Ji, Q.; Zhang, Y.; Gao, T.; Zhang, Y.; Ma, D.; Liu, M.; Chen, Y.; Qiao, X.; Tan, P.-H.; Kan, M., Epitaxial Monolayer MoS_2 on Mica with Novel Photoluminescence. *Nano Lett.* **2013**, *13*, 3870-3877.

34. Dumcenco, D.; Ovchinnikov, D.; Marinov, K.; Lazic, P.; Gibertini, M.; Marzari, N.; Sanchez, O. L.; Kung, Y.-C.; Krasnozhon, D.; Chen, M.-W., Large-Area Epitaxial Monolayer MoS_2. *ACS Nano* **2015**, *9*, 4611-4620.

35. Chen, L.; Liu, B.; Ge, M.; Ma, Y.; Abbas, A. N.; Zhou, C., Step-Edge-Guided Nucleation and

Growth of Aligned WSe_2 on Sapphire *via* a Layer-over-Layer Growth Mode. *ACS Nano* **2015**, *9*, 8368-8375.

36. Curiotto, S.; Chatain, D., Surface Morphology and Composition of C-, a-and M-Sapphire Surfaces in O_2 and H_2 Environments. *Surf. Sci.* **2009**, *603*, 2688-2697.

37. Huang, J.-K.; Pu, J.; Hsu, C.-L.; Chiu, M.-H.; Juang, Z.-Y.; Chang, Y.-H.; Chang, W.-H.; Iwasa, Y.; Takenobu, T.; Li, L.-J., Large-Area Synthesis of Highly Crystalline WSe_2 Monolayers and Device Applications. *ACS Nano* **2013**, *8*, 923-930.

38. Walters, C.; McCarty, K.; Soares, E.; Van Hove, M., The Surface Structure of α-Al_2O_3 Determined by Low-Energy Electron Diffraction: Aluminum Termination and Evidence for Anomolously Large Thermal Vibrations. *Surf. Sci.* **2000**, *464*, L732-L738.

39. Živković, Ž. D.; Dobovišek, B., Kinetics of Aluminium Hydroxide Dehydration. *J. Therm. Anal. Calorim.* **1977**, *12*, 207-215.

40. Govind Rajan, A.; Warner, J. H.; Blankschtein, D.; Strano, M. S., Generalized Mechanistic Model for the Chemical Vapor Deposition of 2D Transition Metal Dichalcogenide Monolayers. *ACS Nano* **2016**, *10*, 4330-4344.

41. Shang, S.-L.; Lindwall, G.; Wang, Y.; Redwing, J. M.; Anderson, T.; Liu, Z.-K., Lateral Versus Vertical Growth of Two-Dimensional Layered Transition-Metal Dichalcogenides: Thermodynamic Insight into MoS_2. *Nano Lett.* **2016**, *16*, 5742-5750.

42. Yang, X.; Li, Q.; Hu, G.; Wang, Z.; Yang, Z.; Liu, X.; Dong, M.; Pan, C., Controlled Synthesis of High-Quality Crystals of Monolayer MoS_2 for Nanoelectronic Device Application. *Sci. China Mater* **2016**, *59*, 182–190.

43. Wieting, T.; Verble, J., Infrared and Raman Studies of Long-Wavelength Optical Phonons in Hexagonal MoS_2. *Phys. Rev. B* **1971**, *3*, 4286.

44. Zhang, Y.; Yang, W., Comment on "Generalized Gradient Approximation Made Simple". *Phys. Rev. Lett.* **1998**, *80*, 890.

45. Blöchl, P. E., Projector Augmented-Wave Method. *Phys. Rev. B* **1994**, *50*, 17953.

46. Kresse, G.; Joubert, D., From Ultrasoft Pseudopotentials to the Projector Augmented-Wave Method. *Phys. Rev. B* **1999**, *59*, 1758.

47. Grimme, S.; Antony, J.; Ehrlich, S.; Krieg, H., A Consistent and Accurate Ab Initio Parametrization of Density Functional Dispersion Correction (DFT-D) for the 94 Elements. H-Pu. *J. Chem. Phys.* **2010**, *132*, 154104.

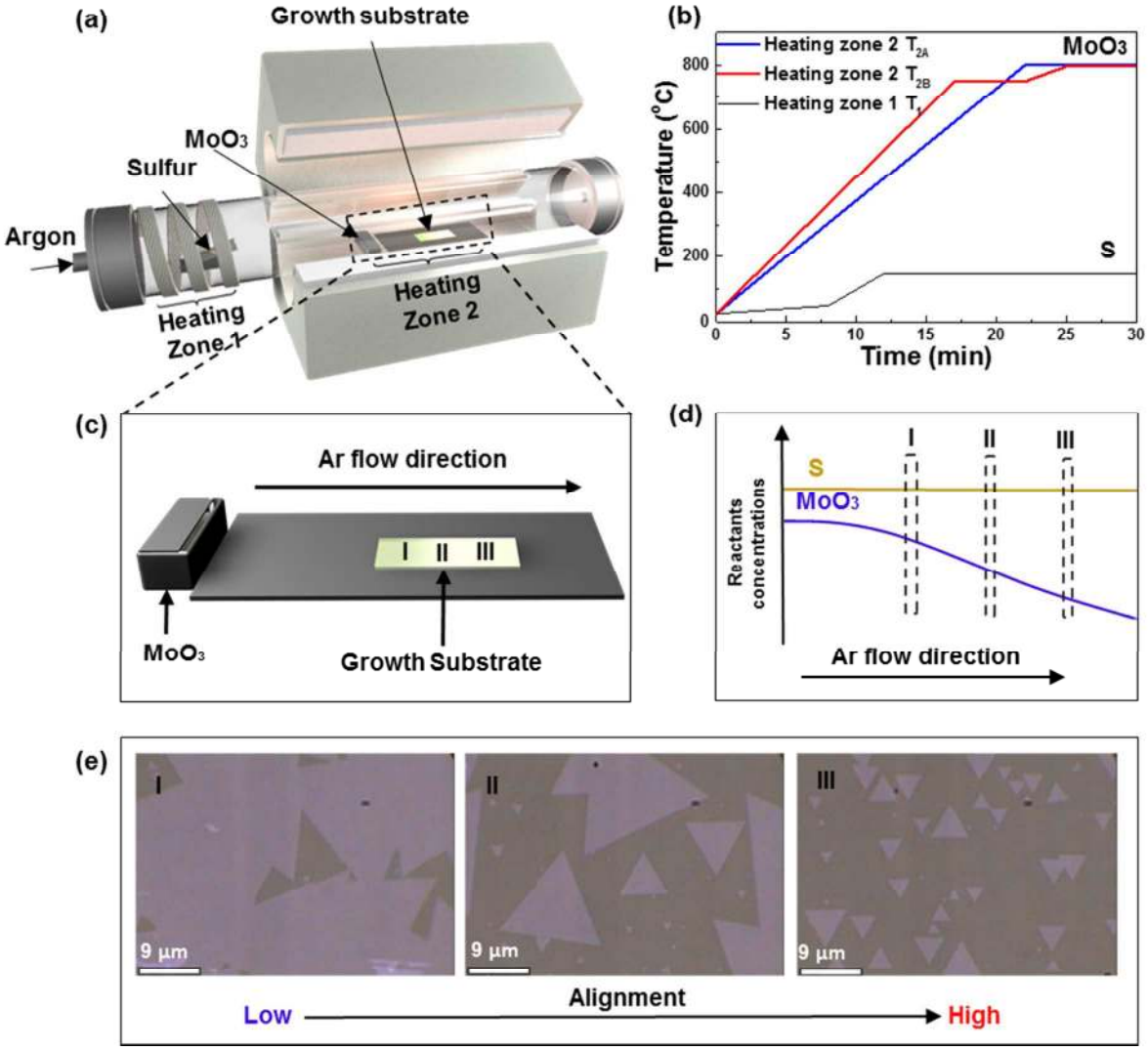

Figure 1. (a) Schematic illustration of the experimental setup of the MoS_2 growth. **(b)** The temperature heating profiles adopted for the study of growing MoS_2. **(c)** Schematic illustration for the various locations (I, II and III) according to the distance away from the MoO_3 source. **(d)** A schematic illustration of the reactants concentration of MoO_3 and S reached the specified locations in (c). **(e)**The corresponding OM images of the MoS_2 flakes at each location. Scale bars: 9 μm.

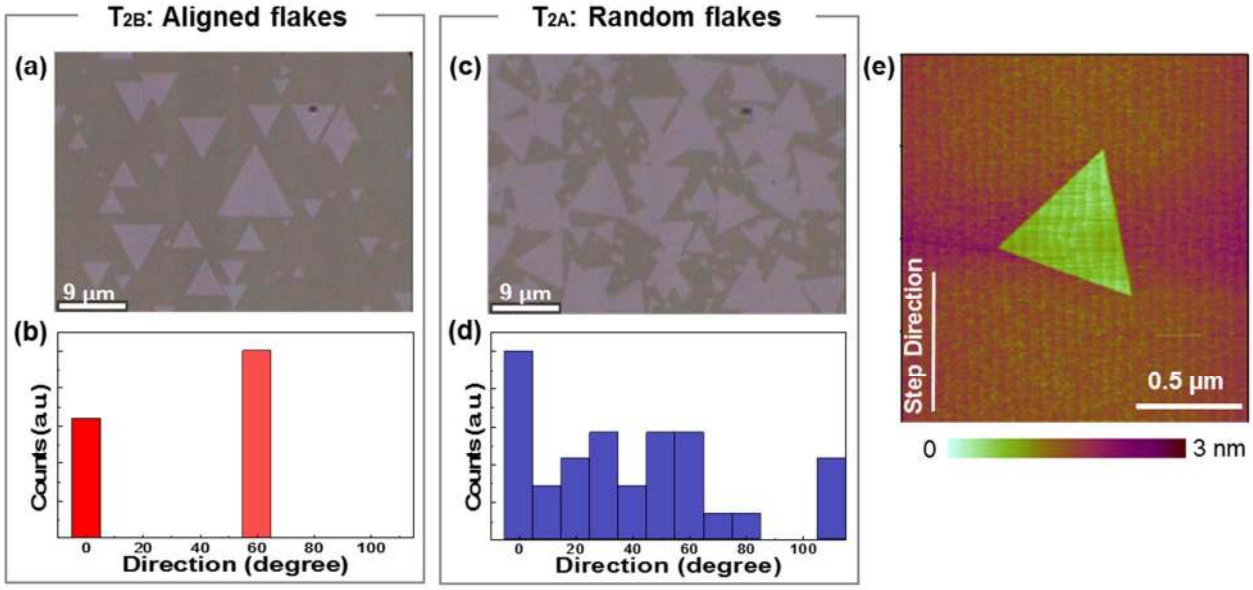

Figure 2. **(a)** The OM image of the as-grown MoS_2 flakes using T_{2B} heating profile. **(b)** Histograms of the orientation distributions based on the image (a). **(c)** The OM image of as-grown MoS_2 flakes using the T_{2A} heating profile. **(d)** Histograms of the orientation distributions based on the image (c). **(e)** AFM image of MoS_2 monolayer flakes grown on c-plane sapphire using T_{2B} heating profile.

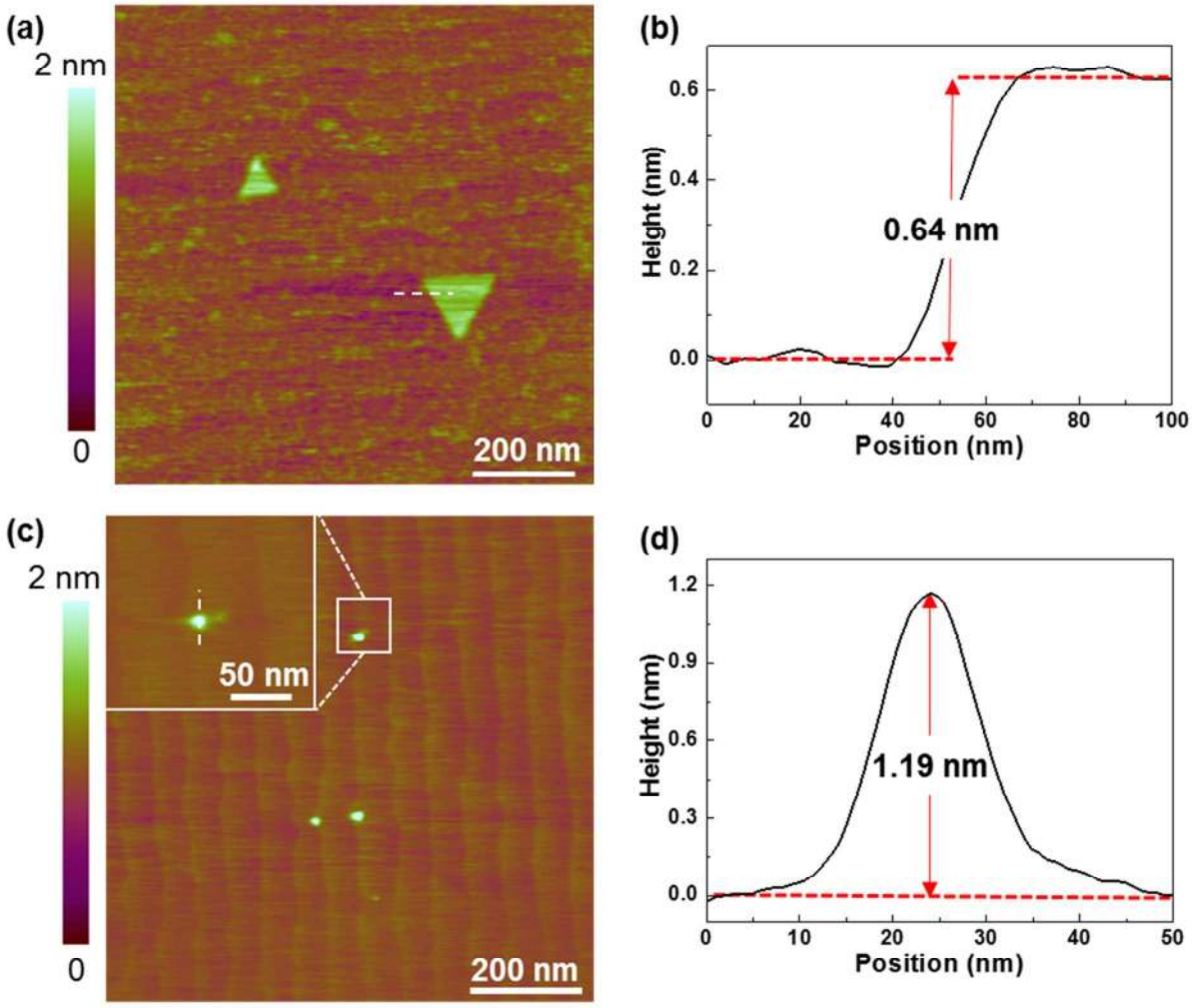

Figure 3. **(a)** AFM image of the MoS_2 seeds at the upstream region. **(b)** Height profile for the white dashed line in (a). **(c)** AFM image of the MoS_2 seeds at the downstream region. The inset in (c) shows zoomed AFM image for the white box. **(d)** Height profile for the white dashed line (c).

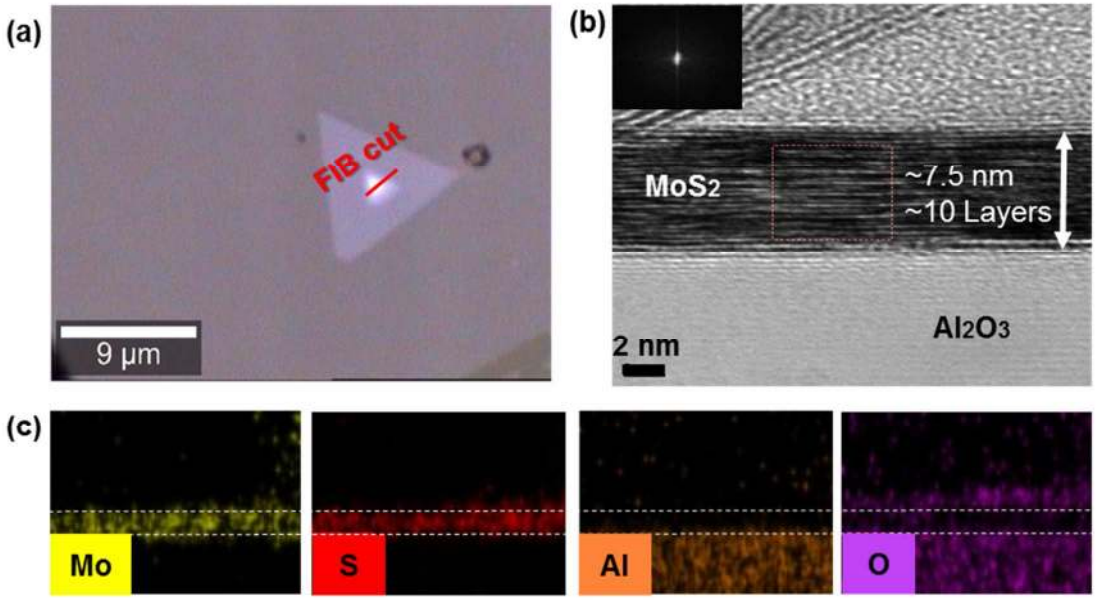

Figure 4. Cross-sectional HRTEM of MoS_2 on c-plane sapphire demonstrating the seed composition. **(a)** The OM image of as-grown MoS_2 flakes with a thick seed. The red line marks the area from which the FIB was cut; **(b)** Cross-sectional HRTEM image of MoS_2 and **(c)** the corresponding EDX maps of (b) for Mo, S, Al and O signals.

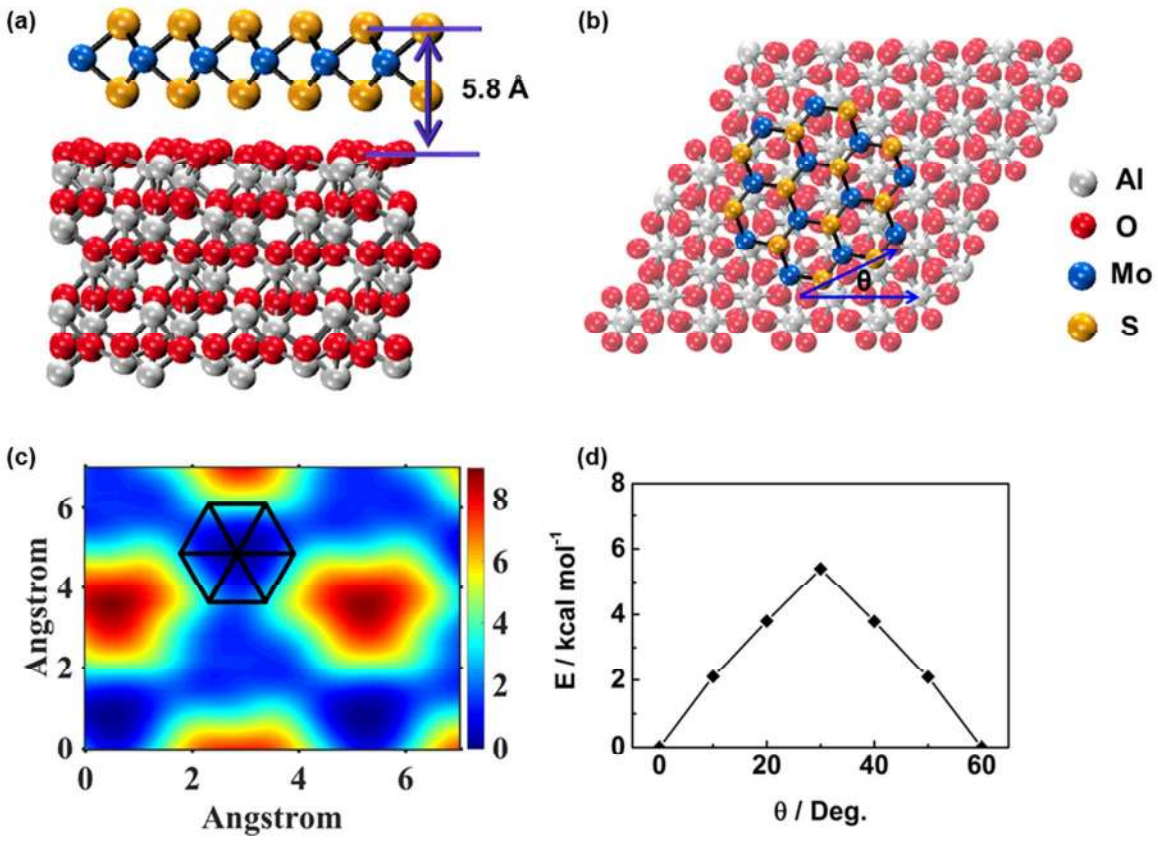

Figure 5. DFT calculation of the relative energy as a function between different orientation angles between MoS_2 seed and sapphire substrate. **(a)** The optimized MoS_2 layer on sapphire substrate demonstrates. **(b)** Schematic view of the MoS_2 hexagon seed on the sapphire substrate. **(c)** Potential energy surface as a function of different relative position of MoS_2 seed on sapphire substrate when the relative angle is fixed as 0. **(d)** Potential energy as a function of relative angle between the MoS_2 seed on sapphire; each configuration was chosen as the minimum point on the position scan (0 degree in c, the rest in supporting information).